DOI: 10.1002/aic.17468

AICHE TOURNAL

Check for updates

FUTURES ISSUE: BIOMOLECULAR ENGINEERING, BIOENGINEERING, BIOCHEMICALS, BIOFUELS, AND FOOD

Silver nanoparticles as an effective antimicrobial against otitis media pathogens

Xiaojing Ma 🕒 Jiayan Lang | Pengyu Chen | Rong Yang ©

Robert F. Smith School of Chemical & Biomolecular Engineering, Cornell University, Ithaca, New York, USA

Correspondence

Rong Yang, Robert F. Smith School of Chemical & Biomolecular Engineering, Cornell University, Ithaca, NY 14850, USA. Email: ryang@cornell.edu

Funding information

National Institute on Deafness and Other Communication Disorders, Grant/Award Number: NIHDC016644; NSF MRSEC program, Grant/Award Number: DMR-1719875

Abstract

Otitis Media (OM) is the most common reason for US children to receive prescribed oral antibiotics, leading to be a potential to cause antibiotic resistance. To minimize oral antibiotic usage, we developed polyvinylpyrrolidone-coated silver nanoparticles (AgNPs-PVP), which completely eradicated common OM pathogens, that is, Streptococcus pneumoniae and nontypeable Haemophilus influenzae (NTHi) at 1.04 and 2.13 µg/ml. The greater antimicrobial efficacy against S. pneumoniae was a result of the H₂O₂-producing ability of S. pneumoniae and the known synergistic interactions between H₂O₂ and AgNPs. To enable the sustained local delivery of AgNPs-PVP (e.g., via injection through perforated tympanic membranes), a hydrogel formulation of 18%(w/v) P407 was developed. Reverse thermal gelation of the AgNPs-PVP-P407 hydrogel could gel rapidly upon entering the warm auditory bullae and thereby sustained release of antimicrobials. This hydrogel-based local delivery system completely eradicated OM pathogens in vitro without cytotoxicity, and thus represents a promising strategy for treating bacterial OM without relying on conventional antibiotics.

KEYWORDS

drug delivery, infectious disease treatment, otitis media, polyvinylpyrrolidone, silver nanoparticles

INTRODUCTION 1

Otitis media (OM), the infection and subsequent inflammation of the middle ear, is the most common illness within the first 24 months of birth. 1 By age 5, over 95% of children in the United States have had at least one episode of OM.^{2,3} In particular, 58% OM episodes are due to bacterial infections caused by gram-positive Streptococcus pneumoniae (S. pneumoniae) and/or gram-negative nontypeable Haemophilus influenzae (NTHi),4,5 pathogens that commonly colonize the nasopharynx and invade the auditory bullae opportunistically to cause OM.6

Oral antibiotic therapy is the current mainstay of treatment for OM. A typical course of treatment comprises 7-10 days of multidose antibiotic regimens. As a result, OM represents the most common reason for pediatric antibiotic prescriptions written to U.S. children.^{2,3}

The level of systemic antibiotic exposure caused by OM is further exacerbated by identified antibiotic resistance of OM pathogens. For example, S. pneumoniae, responsible for over 30% of all OM cases, is known to have greater tolerance for ß-lactam and macrolide.^{8,9} Even with effective fluoroquinolones such as ciprofloxacin, the minimum inhibitory concentration (MIC) of S. pneumoniae is as high as 0.5-4 µg/ml. 10,11 Effective eradication of S. pneumoniae OM requires high antibiotic concentrations in the middle ear, sustained throughout the treatment by adhering to the rigorous multidose oral regimens. The high levels of systemic antibiotic exposure often cause side effects, such as diarrhea, vomiting, and oral thrush, 12 which in turn make it challenging to continue the treatment and potentially lead to recurrent OM and widespread antibiotic resistance.

In this report, silver nanoparticles (AgNPs) were examined as a potential treatment for the OM pathogens. Contrary to small-molecule antibiotics, we found AgNPs (stabilized with polyvinylpyrrolidone [PVP]) to be high efficacious against S. pneumoniae, with MICs lower than that of NTHi, showing a great potential as a broad-spectrum therapy for OM. In recent years, AgNPs have become an attractive alternative to antibiotics due to their excellent antibacterial effects against both grampositive and gram-negative pathogens¹³ and even bacteria with multidrug resistance.¹⁴ Several mechanisms have been considered to explain the antimicrobial efficacy of AgNPs. 15 In brief, AgNPs have been observed to attach to the cell membrane of bacteria, leading to critical damages such as membrane penetration and disabled membrane functions such as respiration (due to deactivation of membrane-bound essential enzymes such as respiratory chain dehydrogenases), 16,17 which in turn increases bacterial membrane permeability. 18,19 AgNPs that penetrated a bacterial cell can damage DNA and deactivate intracellular enzymes. 18,20 leading to rapid cell death. 21 Furthermore, AgNPs are known to generate reactive oxygen species (ROS) including superoxide anion (O2 •-), hydroxyl radical (OH •), and hydrogen peroxide (H₂O₂).²² The excess ROS produced by AgNPs often deplete glutathione (GSH), an antioxidant produced by virtually all living organisms, 23,24 and subsequently damage cell membrane and intracellular organisms. 23,24 Nevertheless, AgNPs have been demonstrated to cause minimal cytotoxicity or immunological responses²⁵ and have thus been adopted across a range of biomedical applications, including drug delivery (e.g., wound healing, 26 eye infection caused by Pseudomonas aeruginosa,²⁷ and postcardiac surgery mediastinitis²⁸) and medical imaging (e.g., human oral cancer²⁹ and multimodality cancer³⁰). Although efficacy of AgNPs against OM pathogens has not been studied previously, we hypothesized that AgNPs could be highly potent, especially against the resistant bacteria S. pneumoniae. That hypothesis was based on the potential synergistic interactions between AgNPs and H₂O₂ due to their Fenton-like reactions and the H2O2-generating ability of S. pneumoniae. 31-33

A hydrogel delivery system was designed to enable the localized and sustained presence of AgNPs during the course of the treatment. This design enables an AgNPs-containing formulation to be administered through a perforated tympanic membrane as a liquid, which quickly turns into a firm solid gel to achieve sustained antimicrobial effects. Reverse thermal gelation, the property that enables liquid-phase administration of the formulation at room temperature and rapid gelation at elevated temperature (e.g., body temperature), was achieved using poloxamer 407 (P407).34,35 It enables a single-dose administration into the middle ear with ease and, once in place, prolonged presence of the formulation to prevent recurrent OM. Furthermore, P407 has been tested as mucoadhesive formulations in rectal delivery of a range of therapeutics such as tizanidine HCI (TIZ) (for treatment of spasticity),³⁶ Ibuprofen (for treatment of pain, fever, rheumatoid arthritis, and osteoarthritis),³⁷ and quinine in children³⁸ (for treatment of malaria), in the nasal delivery of selegiline hydrochloride (for treatment of Parkinson's disease)³⁹ and opiorphin⁴⁰ (for treatment of acute and chronic pain), and vaginal delivery of itraconazole⁴¹ and clotrimazole⁴² (for treatment of vaginal candidiasis). No observable irritation to the mucosal membrane has been observed, 43 hinting at the compatibility of P407-based formulations with the middle ear mucosa. Furthermore,

delivery of OM treatments through a perforated tympanic membrane is particularly applicable to OM patients with recurrent episodes. A recent study showed 54.85% chronic OM cases are accompanied by tympanic membrane perforations,⁴⁴ whereas among children with recurrent AOM 92% had tympanic membrane perforations.⁴⁵ Therefore, the AgNPs reported here have the potential to enable a single-dose and sustained treatment for OM.

In this report, we obtained stable AgNPs colloidal solutions by reducing Ag⁺ in the presence of stabilizer PVP. The as-synthesized particles were approximately 10 nm in diameter, as demonstrated using DLS and TEM. Upon successful demonstration of their antimicrobial efficacy in vitro using *S. pneumoniae*, NTHi, and *Streptococcus mutans* (*S. mutans*) and biocompatibility using human dermal fibroblast (hFBs) and PC-12 Adh cell line (a pheochromocytoma cell line used to test neurotoxicity), the particles were further incorporated in an 18% (w/v) P407 aqueous solution, yielding a hydrogel with reverse thermal gelation temperature at around 25°C. The hydrogel maintained high antimicrobial efficacy and biocompatibility. Therefore, the formulation reported here has the potential to eradicate bacterial pathogens of OM without antibiotics, which circumvents the systemic antibiotic exposure and associated harmful side effects caused by the current oral antibiotic therapy in OM treatment.

2 | EXPERIMENTAL SECTION

2.1 | Nanoparticles synthesis

The stabilized PVP-coated silver nanoparticles (AgNPs-PVP) were synthesized by a chemical reduction reaction as described in the literature. In short, 7.5 ml of an aqueous solution of 1 mM silver nitrate (AgNO₃, 99.9% trace metals basis, Sigma, USA) and 3.75 ml of an aqueous solution of 1 mM PVP (MW 40000, Sigma, USA) were dissolved in deionized (DI) water separately and stirred on a magnetic stir plate until the solutions became homogeneous. Then AgNO₃ and PVP solutions were added together and stirred for 30 mins at 0°C, meantime 18.75 ml of an aqueous solution of 0.2 mM sodium borohydride (NaBH₄, \geq 98.0%, Sigma, USA) was dissolved in DI water at 0°C in a separate flask as a reducing agent for nanoparticles synthesis. Next, the reducing agent solution was added dropwise into the AgNO₃-PVP mixture solution to reduce the Ag⁺-PVP to AgNPs-PVP with the final concentration of 0.25 mM.

The method used to determine the concentrations of the nanoparticles was based on an established approach reported in the literature. In short, because an enough amount (0.7-2 folds that of the concentration of $AgNO_3$) of reducing agent (NaBH₄) was used to obtain AgNPs-PVP and unprotected AgNPs, the reaction conversion with respect to Ag was considered complete and thus the concentration of AgNPs was taken to be the same as the initial concentration of AgNO₃ (i.e., the concentration prior to the addition of NaBH₄). The final molarity concentration ratio of Ag:PVP:NaBH₄ = 2:1:1.4 was chose based on the good stability of as-synthesized AgNPs-PVP in previous reports. The color of the mixture solution became transparent bright yellow indicating formation of AgNPs-PVP.

2.2 | Characterization of AgNPs and AgNPs-PVP

Optical absorbance of AgNPs and AgNPs-PVP was monitored using a UV–Vis Spectrophotometer (Infinite® M1000 PRO) as a function of wavelength in the range from 300 to 500 nm. The incorporation of PVP was proven by a Bruker Vertex V80V Vacuum Fourier Transform Infrared Spectroscopy system (FTIR) in the range of 600–2100 cm⁻¹. The structures and sizes of nanoparticles were observed by 200 kV field emission Transmission Electron Microscopy (FEI F20 TEM/STEM) and Zetasizer (Nano 90) Dynamic Light Scattering (DLS). TEM showed images of particle size and shape on dried carbon-coated copper grid, and DLS gave the particle size in nanoparticle suspension solution.

2.3 | Antibacterial efficacy of AgNPs and AgNPs-PVP

Two gram-positive bacteria, *Streptococcus pneumoniae* (*S. pneumoniae*) and *Streptococcus mutans* (*S. mutans*), and one gram-negative bacteria, nontypeable *Haemophilus influenzae* (NTHi), were chosen to test antibacterial effects of AgNPs-PVP. In short, *S. mutans* was cultured in Brian Heart Infusion (BHI) broth (BD Bioscience, USA), and both *S. pneumoniae* and NTHi were cultured in BHI medium with defibrinated horse blood and nicotinamide adenine dinucleotide (NADH) in a humidified 5% CO₂-conatining balanced-air incubator at 37°C according to established protocols.^{48–50}

The suspension assay for estimation of the minimum inhibitory concentration (MIC) values was carries out to evaluate the antibacterial activity. The MIC values were determined on 96-well plates. Bacteria were cultured to serial dilutions of the AgNPs-PVP or AgNPs (3.125, 6.25, 12.5, 25, 50, and 100 μ M), and the end time points were determined when control group (bacteria only) grew to the stationary phase. Background from the nanoparticles alone was subtracted from the final reading. All assays were carried out in triplicates. All bacterial growth status were monitored by optical density at a wavelength of 600 nm (OD₆₀₀) using a UV–Vis Spectrophotometer (Infinite® M1000 PRO).

2.4 | Hydrogel formation and characterization

Hydrogel formulations were made by adding powdered poloxamer 407 (P407) to DI water and stirring the solution at 4°C until all powder was dissolved to form a clear solution. AgNPs-PVP was then added to the formulated P407 hydrogel solution and stirred until the solution became homogeneous. The hydrogel formulation was referred to as $X\mu$ M[AgNPs-PVP]-18%[P407], where X indicates AgNPs-PVP concentration and 18% is weight per volume concentration of P407. Gelation temperature ($T_{\rm gel}$), storage (G') and loss (G'') modulus were quantified using linear oscillatory shear rheology measurements (1 rads⁻¹, 1% strain, and 1°C/min) by TA Instruments DHR3 Rheometer. $T_{\rm gel}$ is taken as the temperature when the G' became 2 kPa larger than the G''. The changes of G' and G'' were recorded in the temperature range of 20–40°C.

2.5 | *In vitro* release kinetics of hydrogel formulations

The release of AgNPs-PVP from the hydrogel formulations was detected using a similar diffusion system as described in the literature. 51 Transwell membrane inserts (3-μm pore size and 1.1 cm² area; Costar, USA) and 24-well plates were used as the donor and acceptor cells, respectively. A 200 µl aliquot of the formulation containing 18% P407 and 50 or 100 μM AgNPs-PVP was pipetted onto the prewarmed inserts' membrane to get a solid-like hydrogel. Transwell inserts with solid-like hydrogel were placed into the 24-well plates with each well containing 1000 µl prewarmed phosphate-buffered saline (PBS). Then the plates were incubated at 37°C. The 1000 μl aliquots of the PBS were collected at each time point (0.5, 1, 3, 6, 24, and 48 hours), and the inserts were moved to a new well with 1000 ul fresh and prewarmed PBS. Collected aliquots were analyzed with UV-Vis Spectrophotometer; a standard curve was made to determine the AgNPs-PVP concentrations. Experiments were performed in triplicates.

2.6 | Biocompatibility evaluation of AgNPs, PVP, AgNPs-PVP, and hydrogel formulations

The PC-12 cell line (ATCC CRL-1721.1) was cultured with F-12 K medium supplemented (Corning, USA) with 2.5% fetal bovine serum (Gibco, USA), 15% horse serum (Gibco, USA) and 1% penicillin and streptomycin (Gibco, USA). The primary dermal fibroblast cell line (ATCC PCS-201-012) was cultured using the Fibroblast Growth Kit-Low Serum (ATCC PCS-201-041). Both cell lines are maintained in a humidified 5% $\rm CO_2$ -containing balanced-air incubator at 37°C.

Following established protocols, 52,53 the cells used in the cytotoxicity assays were cultured using 96-well plates for assessment of the biocompatibility of AgNPs and AgNPs-PVP, and 24-well plates for hydrogel formulations, respectively. The cells were seeded at the densities of 1×10^4 cells per well in 96-well plates and 4×10^4 cells per well in 24-well plates, respectively, and overnight at 37°C in a humidified 5% CO₂-containing atmosphere. After that, the media in each well was discarded. In 96-well plates, cells were exposed to the AgNPs-PVP and unprotected AgNPs at concentrations of 3.125, 6.25, 12.5, 25, 50, and 100 µM (dissolved in fresh medium) for 24 and 48 hours. In 24-well plates, cells were exposed to the hydrogel formulation containing 18% P407 and AgNPs-PVP at the concentrations of 3.125, 6.25, 12.5, 25, 50, and $100 \,\mu\text{M}$. Viability of the treated or untreated cells were quantified using the CCK-8 kit for mammalian cells (Dojindo Molecular Technologies, Japan). The absorbance at 450 nm was measured after incubating cells with the CCK-8 kit reagents for 1-2 hours. Empty wells with CCK-8 assay reagents only were used as blanks and were subtracted from the final reading. Relative cell viability was calculated by normalizing the absorbance readings using that of untreated cells. All assays were carried out in quadruplicates.

2.7 | Antibacterial test of hydrogel formulations

The surface antibacterial assay was chosen to assess the antibacterial efficacy of the hydrogel formulations based on established approaches reported in previous studies. 54,55 500 µl of 100 µM [AgNPs-PVP]-18%[P407] was pipetted into a 5-ml round bottom tube and stored at 37°C until the formulations became solid-like gel. Next, the 500 µl of prewarmed bacterial broth was added into the tube. The tube was subsequently incubated at 37°C in a humidified 5% CO₂-containing atmosphere for 24 hours. At the end of the incubation, 100 µl suspension was spread onto appropriate agar plates following the spread plates technology and incubated for 24 hours before colony forming units were counted.

3 | RESULTS AND DISCUSSION

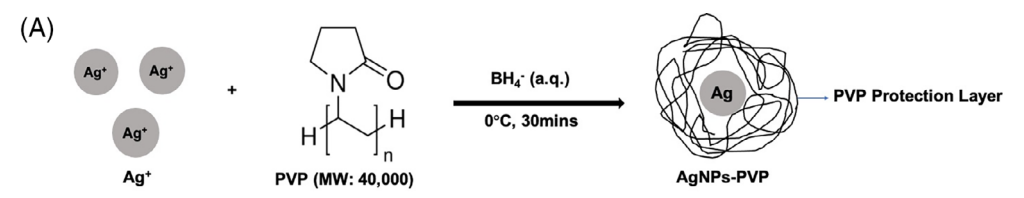
3.1 | Synthesis and characterization of AgNPs-PVP and unprotected AgNPs

AgNPs were synthesized via the commonly adopted approach of reducing silver ions (Ag $^+$) in the presence of a polymeric stabilizer (Figure 1A). 56 Sodium borohydride (BH $_4$ $^-$) was used as the reducing agent 57 because of its rapid reaction with Ag $^+$ and room-temperature

reaction conditions. Ag⁺ and BH₄⁻ quickly reacted to produce AgNPs following the equation below⁴⁶:

$$Ag^{+} + BH_{4}^{-} + 3H_{2}O \rightarrow Ag + H_{3}BO_{3} + 7/2H_{2}$$
 (1)

As-synthesized AgNPs are prone to aggregation, driven by changes in pair potential as a result of the spontaneous hydrolysis of BH₄⁻ and production of sodium hydroxide and orthoborate ([BO₃]³⁻).^{46,58} To prevent the aggregation of AgNPs and control their sizes, PVP was used due to its strong interaction with Ag+, which slowed down the growth of silver grains. And the distance between the resulting silver particles is larger that of the silver particles without PVP⁵⁹). Compared to other stabilizers, such as polyvinyl alcohol (PVA).⁶⁰ PVP demonstrated greater size-regulating capability, likely due to its stronger affinity to Ag⁺ (e.g., the hydroxyl groups in PVA led to weaker interaction than that of Ag⁺-PVP⁶¹ and cellulose⁶² merely acted as a matrix for controlled diffusion of Ag+63). FTIR spectra of PVP and AgNPs-PVP both showed a pronounced peak at 1640 cm⁻¹, indicating C=O stretching and thus presence of PVP. Furthermore, the FTIR spectra of unprotected AgNPs and AgNPs-PVP both showed a peak at 1060 cm⁻¹, representing O-H vibration and presence of AgNPs. Therefore, the spectrum of AgNPs-PVP indicated that the characterizations of both AgNPs and PVP were fully retained in AgNPs-PVP (Figure 1B).



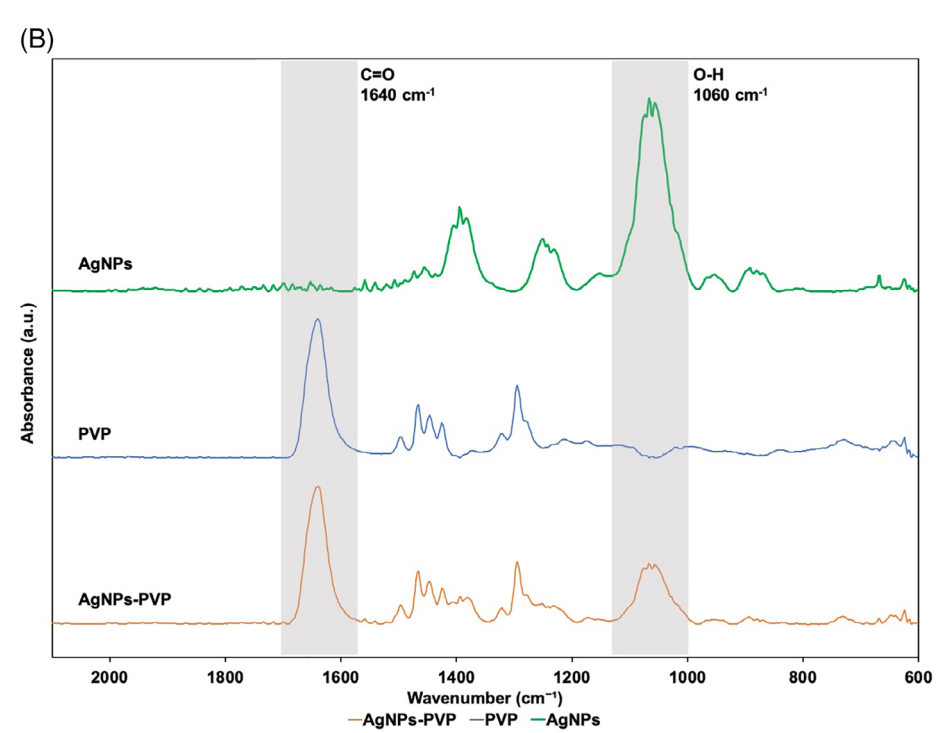


FIGURE 1 Synthesis and FTIR characterization of AgNPs-PVP. (A) AgNPs-PVP was synthesized with the final molarity concentration ratio of Ag:PVP:NaBH₄ = 2:1:1.4 by using NaBH₄ as a reducing agent and PVP as a protection layer. (B) FTIR spectra of AgNPs, PVP, and AgNPs-PVP, demonstrating AgNPs-PVP retained peaks from both of AgNPs (O-H at around 1060 cm⁻¹) and PVP (C=O at around 1640 cm⁻¹)

Sizes of the AgNPs-PVP and unprotected AgNPs were characterized using DLS and TEM. For an aqueous solution of AgNPs-PVP (0.25 mM; AgNPs:PVP = 2:1) (Figure 2A), DLS indicated a narrow range of size distribution, with an average diameter of 9.23 ± 2.03 nm and polydispersity index (PDI) of 0.149. In contrast, DLS captured a much broader size distribution for an aqueous solution of unprotected AgNPs (0.25 mM) due to aggregation, with an average diameter of 31.55 ± 7.9 nm and PDI of 0.336. TEM images further provided direct evidence of the effect of PVP on preventing the aggregation of AgNPs (Figure 2B). While AgNPs-PVP demonstrated a spherical morphology with an average diameter of 10.54 ± 3.11 nm (Figure 2B,D), substantial aggregation was captured for unprotected AgNPs (Figure 2B). The characteristic length of the aggregates was calculated to be 25.82 ± 11.98 nm (Figure 2C), obtained by processing TEM images using ImageJ. The fact that DLS measured an average diameter greater than that captured by TEM is well documented in the literature. 64,65 It has been attributed to the hydrodynamic diameter (as measured by DLS) being greater than the projected area diameter (as captured by TEM), due to a solvent layer surrounding a colloid that are subject to the particle Brownian motion.

Upon dispersion in water at the concentration of 0.25 mM, AgNPs-PVP formed a stable colloidal solution (Figure 3B), which remained unchanged after 7 days of storage under ambient conditions. The solution exhibited a maximum absorption at 404 nm, as characterized using UV-vis spectrophotometry (Figure 3B, corresponding to the bright yellow color), which also remained unchanged after the 7-day storage. Although a freshly made aqueous solution of unprotected AgNPs (0.25 mM) exhibited a similar color as that of AgNPs-PVP, the absorption peaks at 375 and 425 nm hinted at the polydispersed particle sizes due to aggregation. After 7 days of storage, the solution demonstrated a dark gray color, with no discernable UV-vis absorption (Figure 3A), indicating instability of the solution. The superior stability of AgNPs-PVP solutions likely led to their greater antimicrobial efficacy against OM pathogens, as described below.

3.2 | Antibacterial efficacy of AgNPs-PVP and unprotected AgNPs

As discussed previously, *S. pneumoniae* and NTHi are the two most common bacteria pathogens causing OM, accounting for 58% of the

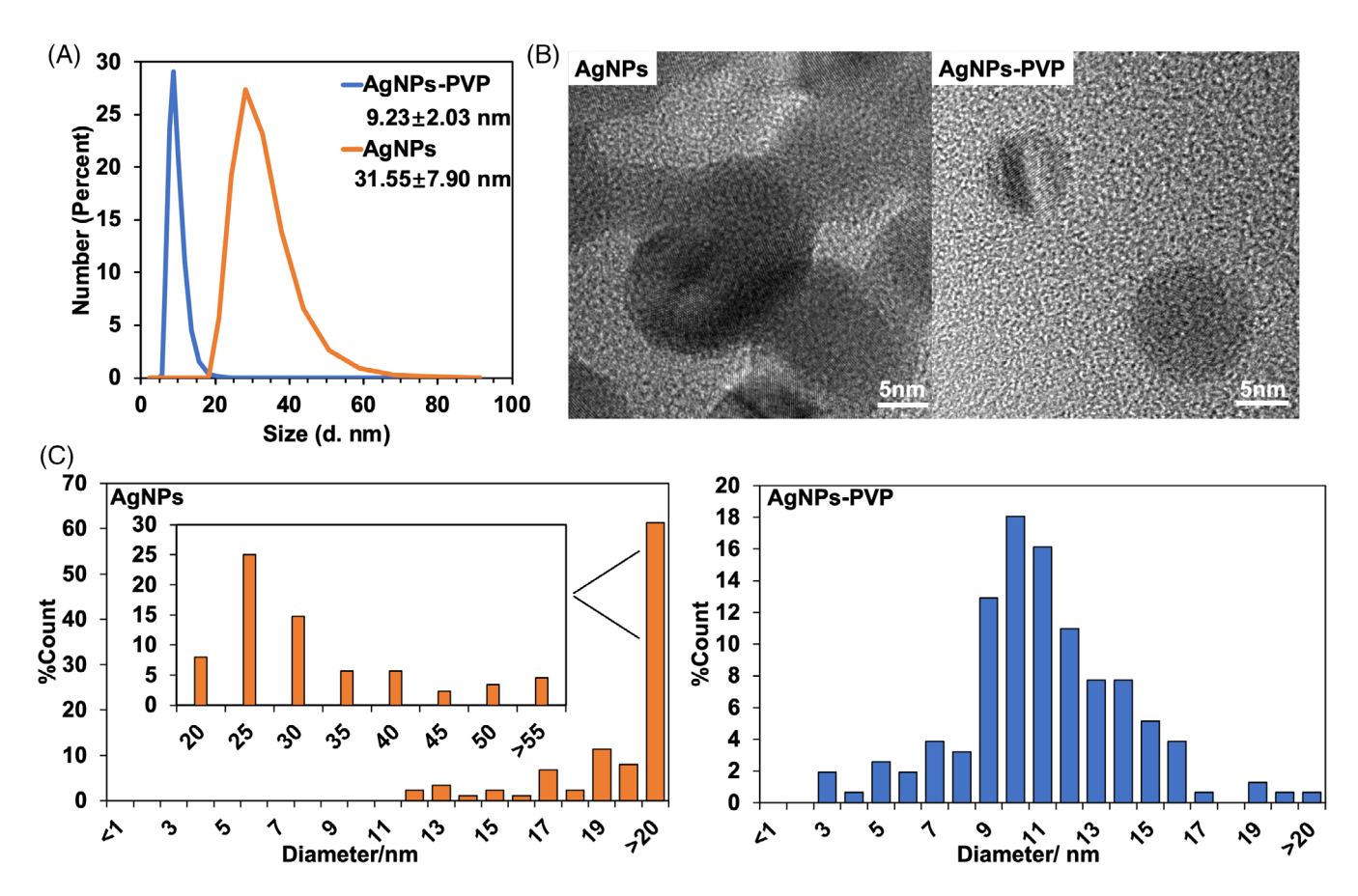


FIGURE 2 DLS and TEM analyses of particle sizes. (A) DLS indicated a narrow size distribution for AgNPs-PVP, with an average diameter of 9.23 ± 2.03 nm and a PDI of 0.149; whereas unprotected AgNPs demonstrated an average diameter of 31.55 ± 7.9 nm with PDI of 0.336. (B) TEM images of unprotected AgNPs and AgNPs-PVP, showing aggregates for the former and regular spherical morphology for the latter. (C) Particle size distributions of unprotected AgNPs (25.82 ± 11.98 nm) and AgNPs-PVP (25.82 ± 11.98 nm) obtained by analyzing TEM images (25.82 ± 11.98 nm) and AgNPs-PVP (25.82 ± 11.98 nm)

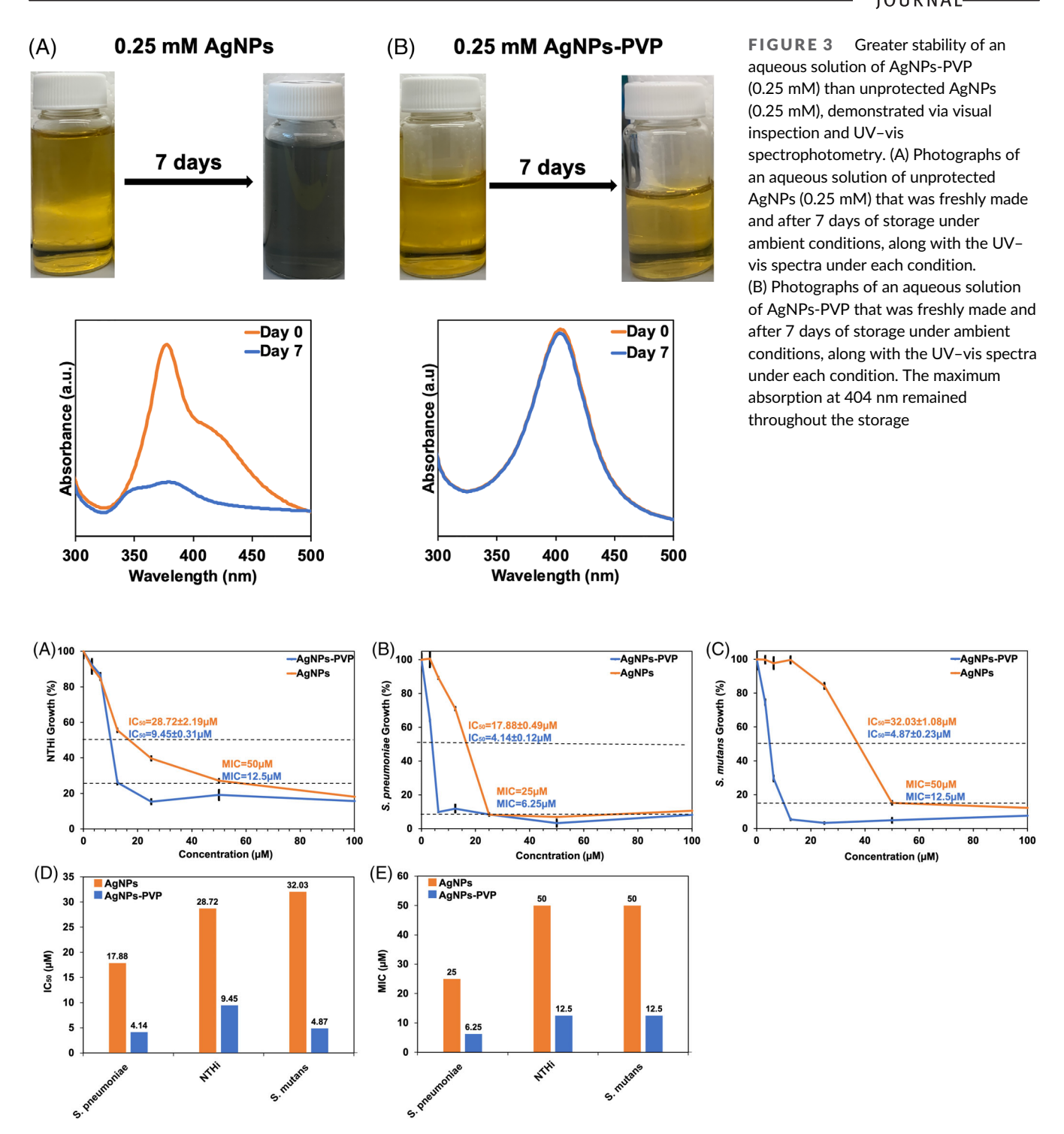


FIGURE 4 Antibacterial effect of unprotected AgNPs and AgNPs-PVP. (A–C) Growth of NTHi (A), *S. pneumoniae* (B), and *S. mutans* (C) after 12 hours of incubation without or with varying concentrations of AgNPs and AgNPs-PVP, normalized by the growth without antimicrobials (i.e., 100% growth represents the growth of bacteria without AgNPs or AgNPs-PVP). MIC and IC₅₀ are indicated with dashed lines. Data are mean \pm SD. (D–E) Summary of IC₅₀ (D) and MIC (E) values of AgNPs and AgNPs-PVP against NTHi, *S. pneumoniae* and *S. mutans.* n=3 for each group

total OM episodes in the United States. ⁵ The antibacterial efficacy of AgNPs-PVP and unprotected AgNPs was thus tested using these two pathogens. The measurement of optical density at 600 nm (OD_{600}) was used to detect bacterial growth based on their light scattering. Despite the prevalence of this approach, it is prone to "false positive"

results because dead cells and cells debris can contribute to the measured scattering, leading to nonzero OD₆₀₀ reading in samples with no viable cells.⁶⁶ The MIC and half maximal inhibitory concentration (IC₅₀) were used to quantify the antibacterial efficacy. MIC was obtained via broth microdilution assay, where MIC corresponds

to the lowest concentration of antimicrobials that prevented bacterial growth. To better characterize the affected bacterial growth before complete eradication (i.e., MIC) was achieved, IC_{50} was calculated, defined as the concentration of antimicrobials that led to a stationary OD_{600} that was half of that without antimicrobials. For antimicrobials with the same MIC, lower IC_{50} indicates higher antimicrobial effect.

The antimicrobial efficacy of AgNPs against NTHi showed an average IC $_{50}$ of 28.72 μ M (\sim 4.88 μ g/ml) and an average MIC of 50 μ M (\sim 8.5 μ g/ml) (Figure 4A). The average values of IC $_{50}$ and MIC were much reduced in the presence of PVP, which became 9.45 μ M (\sim 1.61 μ g/ml) and 12.5 μ M (\sim 2.13 μ g/ml) respectively (Figure 4A). The greater antimicrobial efficacy of AgNPs-PVP than unprotected AgNPs was likely a result of the stabilized particulates (Figure 3) with greater surface-to-volume ratio than aggregates that led to enhanced interactions with pathogens.

The antibacterial efficacy of AgNPs-PVP was comparable to tradition antibiotics against NTHi, such as Amoxicillin (with MIC of 0.5-2 µg/ml), Clarithromycin (with MIC of 2-8 µg/ml), and Azithromycin

(with MIC of 0.25–2 μ g/ml).⁶⁷ Contrary to those small-molecule antibiotics, efficacy of AgNPs and AgNPs-PVP against *S. pneumoniae* was better than that against NTHi (Figure 4B), with IC₅₀ values of 17.88 μ M (~2.99 μ g/ml) and 4.14 μ M (~0.70 μ g/ml) for AgNPs and AgNPs-PVP respective and MIC values of 25 μ M (~4.18 μ g/ml) and 6.25 μ M (~1.04 μ g/ml) for AgNPs and AgNPs-PVP respective. The stronger antimicrobial effects of AgNPs and AgNPs-PVP against *S. pneumoniae* than that against NTHi could be due to their gram types or the known production of H₂O₂ by *S. pneumoniae* (at levels around 0.1–0.71 mM as a mechanism for competitive survival during coinfections).⁶⁸ To better understand this differential efficacy of AgNPs-PVP, *S. mutans*, a gram-positive pathogen (same as *S. pneumoniae*) with much lower activity of H₂O₂ production (at levels around 0–0.06 mM^{69,70}) was tested.

S. mutans is one of the microorganisms inhabiting the oral cavity, which has been studied for its etiology of dental caries and infective endocarditis.⁷¹ Interestingly, the colonization of *S. mutans* in mouth has been shown to be correlated with the colonization of *S. pneumonia* in the nasopharynx,⁷² thus making *S. mutans* a pathogen

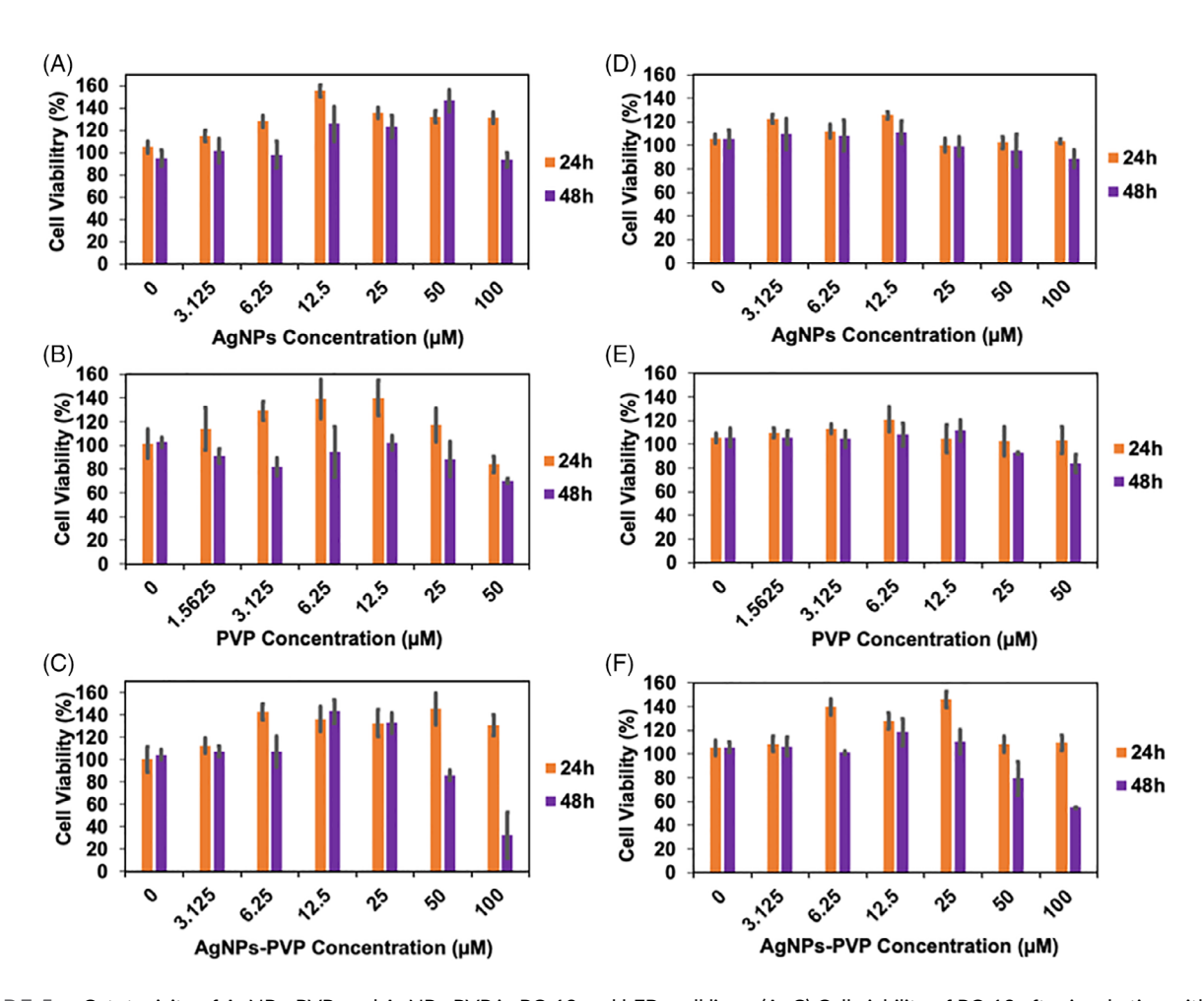


FIGURE 5 Cytotoxicity of AgNPs, PVP, and AgNPs-PVP in PC-12 and hFBs cell lines. (A–C) Cell viability of PC-12 after incubating with different concentrations of AgNPs, PVP, and AgNPs-PVP, at 24 and 48 hours. (D–F) Cell viability of hFBs after incubating with different concentrations of AgNPs, PVP, and AgNPs-PVP, at 24 and 48 hours. Culture of PC-12 or hFBs without any exposure to AgNPs, PVP, or AgNPs-PVP was considered 100% cell viability. Error bars represent SDs. n = 4 for each group

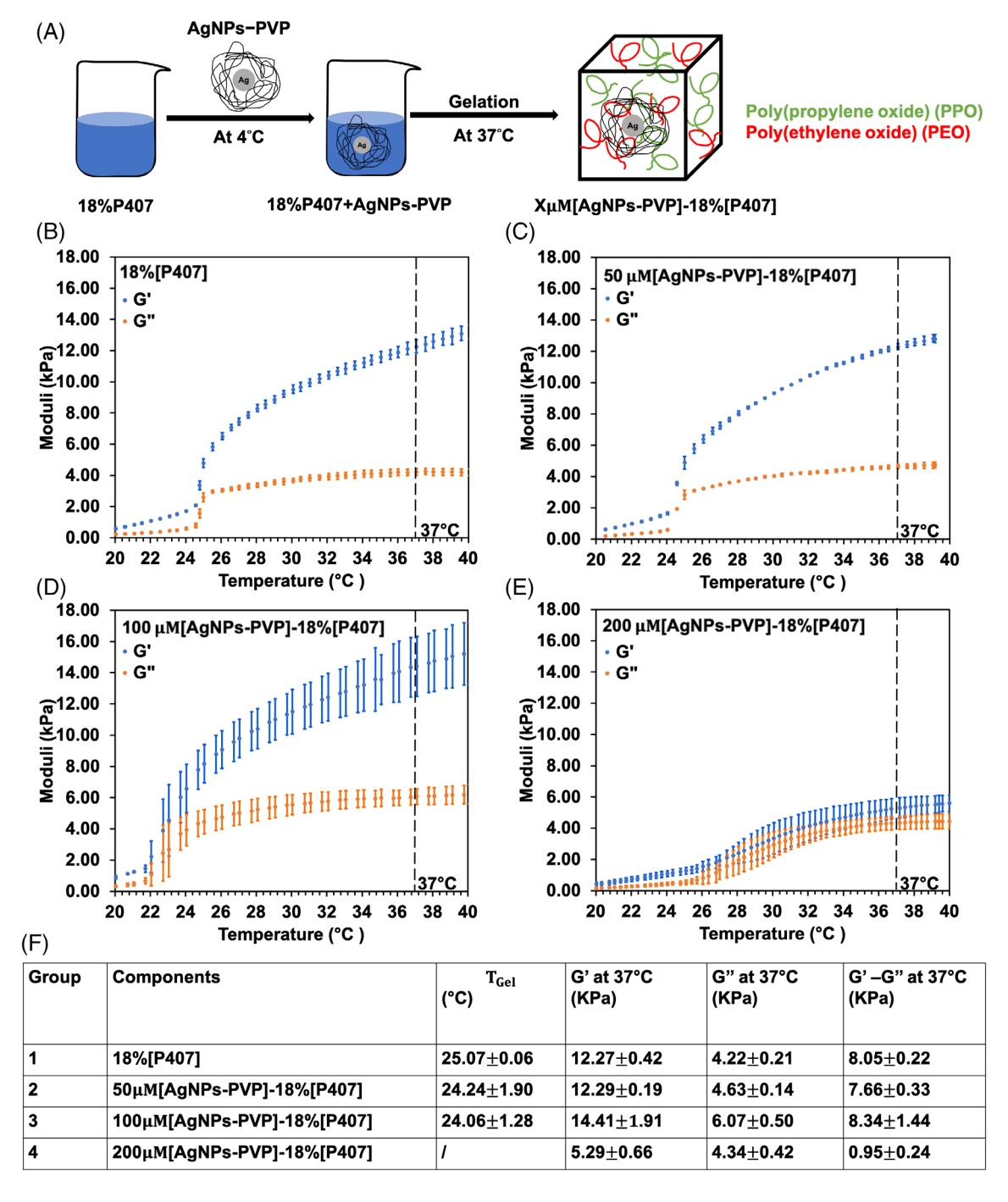


FIGURE 6 Formulation and rheology of the antimicrobial and temperature-responsive hydrogel delivery system. (A) Formulation of the hydrogels. AgNPs-PVP was introduced to an 18%(w/v) aqueous solution of P407 to the final concentrations of 50, 100, and 200 μM, respectively. The formulations were thereinafter referred to as $X\mu$ M[AgNPs-PVP]-18%[P407], where X indicates the concentration of Ag. (B–E) Linear oscillatory shear rheology of the formulations containing 18%[P407] (B), 50 μM[AgNPs-PVP]-18%[P407] (C), 100 μM [AgNPs-PVP]-18%[P407] (D), and 200 μM [AgNPs-PVP]-18%[P407] (E), with dashed lines highlighting the storage modulus (G) and loss modulus (G) at 37°C. (F) Summary of gelation temperatures and values of G1 and G1 at 37°C, for the four aforementioned formulations. Data are mean \pm SD. n=3 for each group

of interest for OM treatment. Indeed, the MIC values of AgNPs and AgNPs-PVP against *S. mutans* were 50 μ M (\sim 8.35 μ g/ml) and 12.5 μ M (\sim 2.09 μ g/ml) respectively, which were comparable to NTHi and greater than *S. pneumoniae* (Figure 4C). Similarly, the IC₅₀ value of AgNPs and AgNPs-PVP against *S. mutans* were 32.03 μ M (\sim 5.35 μ g/

ml) comparable to that of NTHi. The IC₅₀ value of AgNPs-PVP, 4.87 μ M (\sim 0.81 μ g/ml), was smaller than that of NTHi (9.45 μ M [\sim 1.58 μ g/ml]) and close to that of *S. pneumoniae* (4.14 μ M [\sim 0.70 μ g/ml]), which could be explained by the bacteriostatic effect of low levels of H₂O₂ on *S. mutans.*⁷³ Taken together, the MIC and

IC₅₀ values of AgNPs and AgNPs-PVP against *S. mutans* confirmed that their greater efficacy against *S. pneumoniae* was likely a result of the H₂O₂-producing capability and not gram types, as gram-positive *S. mutans* and gram-negative NTHi demonstrated comparable values.

3.3 | Cytotoxicity of AgNPs-PVP and unprotected AgNPs

Cytotoxicity of AgNPs and AgNPs-PVP was evaluated and quantified with the PC-12 Adh cell line and the primary dermal fibroblast cell line (hFBs) using the CCK-8 assay. The PC-12 cell line was chosen to mimic the response of auditory neural cells to the AgNPs and AgNPs-PVP; whereas the hFBs was chosen based on its representation of connective tissues that are prevalent in the TM. The percentage of cell viability was assessed at different concentrations of AgNPs, PVP, and AgNPs-PVP, respectively (Figure 5).

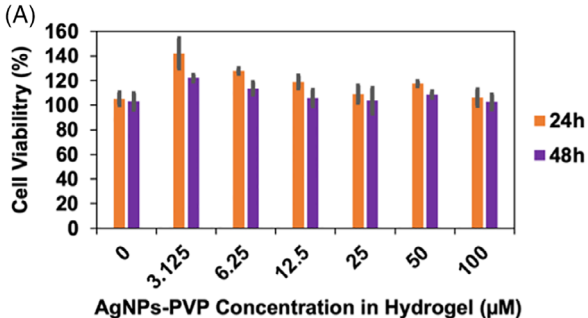
AgNPs showed negligible cytotoxicity in the concentration range of 0-100 μM (far exceeded the MIC for all three pathogens tested) in PC-12 and hFBs cell lines at 24 and 48 hours (Figure 5A,D). Cytotoxicity of PVP alone was assessed in the concentration range of 0–50 μM in both cell lines (Figure 5B,E), corresponding to the range used in the AgNPs-PVP formulations (AgNPs-PVP formulations were made with a 2:1 molar ratio of AgNPs and PVP). PVP also demonstrated minimal cytotoxicity, consistent with the biocompatibility reported in the literature.74 All concentrations of AgNPs-PVP formulations in PC-12 and hFBs demonstrated virtually unchanged cell viability (Figure 5C,F), indicating excellent biocompatibility in 24 hours. At 48 hours, mild cytotoxicity was observed for AgNPs-PVP at the concentrations of 50 and 100 uM (representing the concentrations of AgNPs), with cell viability values of 80% and 20% for PC-12, and 80% and 55% for hFBs, respectively (Figure 5C,F). Nevertheless, the AgNPs-PVP formulation caused no observable cytotoxicity at concentrations at or below the MICs (i.e., 12.5 μM for NTHi and S. mutans and 6.25 μM for S. pneumoniae) in PC-12 and hFBs at both 24 and 48 hours and the formulation was thus considered safe under effective concentrations.

3.4 | Formulation and rheology of the antimicrobial and temperature-responsive hydrogel delivery system

AgNPs-PVP was chosen to formulate the hydrogel delivery system due to its superior antimicrobial efficacy compared to unprotected AgNPs. AgNPs-PVP was added to an 18%(w/v) P407 aqueous solution to formulate the antimicrobial and temperature-responsive hydrogel, with concentration of the AgNPs-PVP (Ag:PVP ratio of 2:1) in the hydrogel varied in the range of 0–100 μ M. The resulting formulation was referred to as X μ M[AgNPs-PVP]-18%[P407], where X indicated the concentration of Ag (Figure 6A).

As discussed previously, P407 was used here due to its reverse thermal gelation properties, that is, the AgNPs-PVP-containing formulation could flow readily into the middle ear space during administration, and then gel promptly at 37° C to ensure sustained antimicrobial effect. The concentration of P407, that is, 18% (w/v), was selected based on our prior experience, which led to a gelation temperature close to 37° C and sufficient gel strength to sustain drug delivery over the 7-10 day course of treatment.⁵¹

Linear oscillatory shear rheology of the AgNPs-PVP-containing hydrogel formulations demonstrated that introduction of the nanotherapeutics at concentrations at or below 100 µM did not jeopardize the desirable reverse thermal gelation. For each formulation, storage (G') and loss (G'') moduli were quantified in the temperature range of 20-40°C; and gelation (i.e., the transition from a liquid formulation to a solid gel) was defined as the point where G' was greater than G" by 2 kPa. Without the nanotherapeutics, the formulation containing 18%[P407] had a gelation temperature of 25°C, and G' and G''of 12.27 ± 0.42 and 4.22 ± 0.21 kPa at 37° C (Figure 6B). At the AgNPs-PVP concentration of 50 μM, the hydrogel formulation demonstrated virtually unchanged gelation temperature of 24°C, and G' and G'' of 12.29 ± 0.19 and 4.63 ± 0.14 kPa, respectively, at 37°C (Figure 6C). With 100 μM AgNPs-PVP, the gelation temperature remained at 24° C, with G' and G'' values increased to 14.41 ± 1.91 and 6.07 ± 0.50 kPa at 37°C (Figure 6D), which was likely a result of the entanglement between PVP and P407 chains. Gelation did not occur for the formulation of 200 μM[AgNPs-PVP]-18%[P407] and G' was reduced to 5.29 ± 0.66 kPa, merely half of that of 18%[P407](Figure 6E). This could be attributed to the inability for P407 chains to



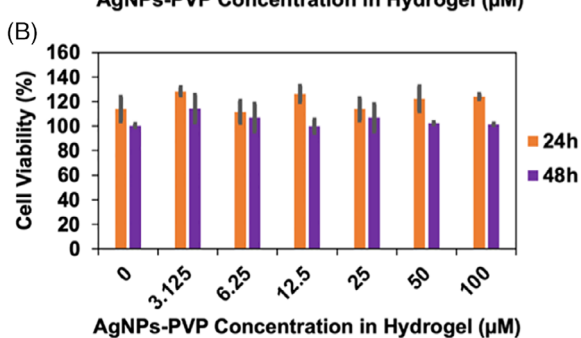


FIGURE 7 Toxicity evaluation of formulations $X\mu$ M[AgNPs-PVP]-18%[P407]. (A) Cell viability of PC-12 after incubating with $X\mu$ M [AgNPs-PVP]-18%[P407] (X=0,3.125,6.25,12.5,25,50, or 100) for 24 and 48 hours. (B) Cell viability of hFBs after incubating with $X\mu$ M [AgNPs-PVP]-18%[P407] (X=0,3.125,6.25,12.5,25,50, or 100) for 24 and 48 hours. Culture of PC-12 or hFBs without any exposure to the hydrogel formulations was considered 100% cell viability. Error bars represent standard deviations. n=4 for each group

form micelles and/or for micelles to pack into a solid gel due to the substantial presence of PVP chains. Values of the gelation temperatures and storage/loss moduli were summarized in a table (Figure 6F).

3.5 | Cytotoxicity of the hydrogel formulations

Cytotoxicity of $X\mu$ M[AgNPs-PVP]-18%[P407] with Ag concentration ranging from 0 to 100 μ M was evaluated using PC-12 and hFBs, the two common cell lines used to assess cytotoxicity of topical formulations. The percentage of cell viability was assessed at different concentrations of AgNPs-PVP in hydrogel (Figure 7).

All formulations of X μ M[AgNPs-PVP]-18%[P407] tested using PC-12 and hFBs showed negligible cytotoxicity at both 24 and 48 hours (Figure 7), indicating excellent biocompatibility. Cytotoxicity was markedly improved for 50 μ M[AgNPs-PVP]-18%[P407] and 100 μ M[AgNPs-PVP]-18%[P407] compared to the aqueous solutions of 50 and 100 μ M AgNPs-PVP (Figure 5C,F). This phenomenon could be attributed to the sustained release and thus controlled dosing of AgNPs-PVP from the hydrogel formulations, effectively reducing the concentration of AgNPs-PVP to which PC-12 and hFBs cells were exposed. The formulations of 50 and 100 μ M[AgNPs-PVP]-18% [P407] were selected for further assessment of in vitro release studies given their excellent biocompatibility.

3.6 | In vitro release of AgNPs-PVP from the hydrogel formulations with reverse thermal gelation

The cumulative release of AgNPs-PVP was studied by quantifying the *in vitro* diffusion of Ag from hydrogel formulations placed in a Transwell[®]. Effect of initial drug loading amount on release kinetics of

the hydrogel formulations was investigated using two hydrogel formulations, 50 μ M[AgNPs-PVP]-18%[P407] and 100 μ M[AgNPs-PVP]-18%[P407]. Consistent with previous reports, 51,75 lower initial drug loading amount resulted in slightly greater cumulative release fraction by the end of the 48 hours testing period (Figure 8). At 3 hours, the two formulations had similarly low release fractions, that is, 5.38 \pm 2.32% for 50 μ M[AgNPs-PVP]-18%[P407] and 2.79 \pm 0.40% for 100 μ M[AgNPs-PVP]-18%[P407]. The total amounts of Ag released from the two formulations were comparable. At 6 hours, 49.49 \pm 1.24% was released from 50 μ M[AgNPs-PVP]-18%[P407] and 44.64 \pm 2.94% from 100 μ M[AgNPs-PVP]-18%[P407], where the amount of Ag released from the latter exceeded that of the former by

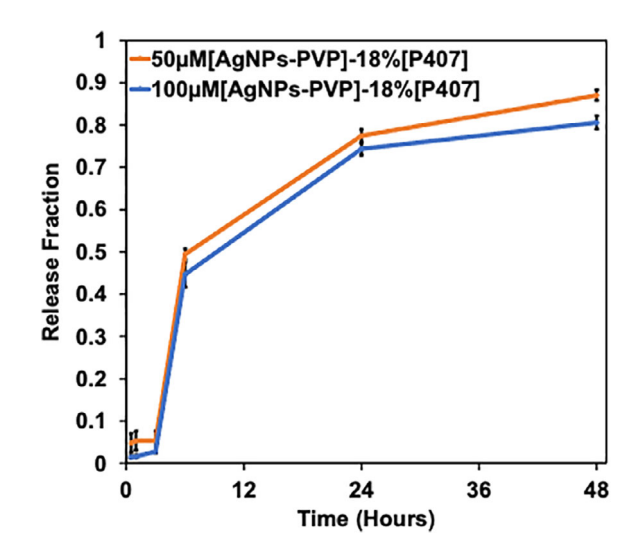


FIGURE 8 Cumulative *in vitro* release of Ag from 50 μ M[AgNPs-PVP]-18%[P407] and 100 μ M[AgNPs-PVP]-18%[P407]. n=3 for each group. Data were mean ± SD

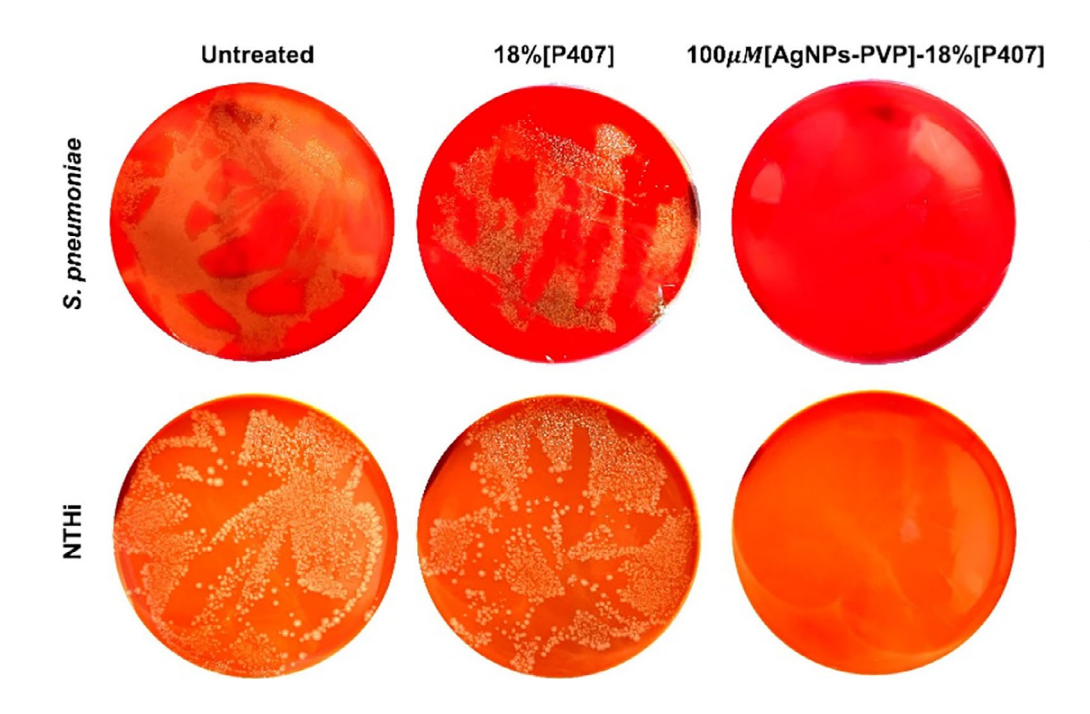


FIGURE 9 Antibacterial efficacy of the hydrogel delivery system tested using S. pneumoniae and NTHi. The 100 μM[AgNPs-PVP]-18%[P407] formulation (500 µl) was stored at 37°C until it became a solid-like gel; prewarmed bacterial broth (500 µl) was subsequently added to the hydrogel. The tube was then incubated at 37°C for 24 hours, by the end of which. 100 μl of the culture was applied on agar plates and incubated for 24 hours. The hydrogel formulation, 100 μM[AgNPs-PVP]-18%[P407] completely eradicated both S. pneumoniae and NTHi

nearly twofold, implying that the release of Ag was dominated by passive diffusion. Similar observations were made at 24 and 48 hours, that is, $50 \,\mu\text{M}[\text{AgNPs-PVP}]-18\%[\text{P407}]$ achieved cumulative release fractions of $77.41 \pm 1.60\%$ and $87.03 \pm 1.25\%$, respectively, and $100 \,\mu\text{M}[\text{AgNPs-PVP}]-18\%[\text{P407}]$ achieved $74.37 \pm 1.56\%$, and $80.61 \pm 1.65\%$, respectively. The cumulative release fractions of $100 \,\mu\text{M}$ [AgNPs-PVP]-18%[P407] were slightly less than twofold that of $50 \,\mu\text{M}[\text{AgNPs-PVP}]-18\%[\text{P407}]$ at 6, 24, and 28 hours, which was likely a result of the aforementioned entanglement between PVP and P407 chains that increased physical cross-linking and reduced rate of passive diffusion.

3.7 | Antibacterial efficacy of the AgNPs-PVP-containing hydrogel

Using the formulation containing the highest concentration of AgNPs-PVP while still maintaining reverse thermal gelation, that is, 100 μ M [AgNPs-PVP]-18%[P407], antimicrobial efficacy was examined. As discussed previously, *S. pneumoniae* and NTHi, the two main pathogens causing OM, ⁵ were used.

To mimic the environment of an auditory bullae during an active episode of OM, which has the volume of 1.52 ± 0.26 ml (mean \pm SD),⁷⁶ 500 μl hydrogel formulation was applied to 500 μl bacteria broth and incubated for 24 hours. The antibacterial activity of hydrogel formulations was assessed by counting the colony-forming unites (CFU) at the end of the 24-hour incubation (Figure 9). The method of applying bacterial culture directly onto the surface of hydrogel formulations has been widely used in previous reports to assess antimicrobial efficacy, 52,77-80 and have demonstrated excellent correlation with in vivo efficacy results. This method was adopted here instead of applying the hydrogel using Transwell membrane inserts (like those used in the in vitro release studies) also because the inserts alone were discovered to inhibit the bacterial growth and interfere with the antimicrobial efficacy results (Figure S6). While countless colonies of S. pneumoniae and NTHi were observed on the agars that were untreated or treated with 18%[P407], 100 µM[AgNPs-PVP]-18%[P407] achieved complete eradication of both pathogens, demonstrating the potential of this local treatment to cure OM with high bacterial counts.

4 | CONCLUSION

In summary, we designed a hydrogel formulation (100 μ M[AgNPs-PVP]-18%[P407]), which achieved complete eradication of the two most common bacterial OM pathogens, that is, *S. pneumoniae* and NTHi *in vitro* without causing cytotoxicity. The AgNPs-PVP was synthesized via a chemical reduction reaction using NaBH₄ as the reducing agent and PVP as the stabilizer. The as-synthesized AgNPs-PVP demonstrated a narrow size distribution (\sim 10 nm), which led to their effective eradication of the bacterial OM pathogens at MIC values of 6.25 μ M (\sim 1.04 μ g/ml) for *S. pneumoniae* and 12.5 μ M (\sim 2.13 μ g/ml) for NTHi. To realize the local and sustained delivery of the AgNPs-PVP, a hydrogel with reverse thermal gelation properties was

formulated, promising a delivery system with ease of administration through (perforated) tympanic membranes and sustained presence in the auditory bullae. Gelation temperature of the final hydrogel formulation, 100 μ M[AgNPs-PVP]-18%[P407], was measured to be 24.06 \pm 1.28°C using linear oscillatory shear rheology. The antimicrobials released from 100 μ M[AgNPs-PVP]-18%[P407] eradicated the two aforementioned OM pathogens without triggering cytotoxicity. The hydrogel formulations were designed to provide sustained release of the AgNPs-PVP for the duration of the treatment, which has been shown to be necessary for the clearance of the infection. 51 This was the first time that AgNPs were used against OM pathogens, and the hydrogel formulation thus points to an effective and biocompatible solution to treat OM while circumventing the health concerns associated with systemic antibiotic exposure.

ACKNOWLEDGMENTS

The authors acknowledge the National Institutes of Health - National Institute on Deafness and Other Communication Disorders for support (NIHDC016644 to Rong Yang). Analytical methods involved use of the Cornell Center for Materials Research (CCMR) Shared Facilities which are supported through the NSF MRSEC program (DMR-1719875). Authors thank J. Grazul for support TEM preparation.

CONFLICT OF INTEREST

The authors declare no competing financial interest.

AUTHOR CONTRIBUTION

Xiaojing Ma: Writing-original draft (equal); Jiayan Lang: Writing-original draft (equal); Pengyu Chen: Formal analysis (supporting); Rong Yang: Supervision (lead).

DATA AVAILABILITY STATEMENT

The authors declare that the main data supporting the findings of this study are available within the article and its Supplementary Materials files. Extra data about this study are available from the corresponding author upon request.

ORCID

Xiaojing Ma https://orcid.org/0000-0002-3584-0769
Rong Yang https://orcid.org/0000-0001-6427-026X

REFERENCES

- Paul Caroline R, Moreno Megan A. Acute Otitis Media. JAMA Pediatrics. 2020;174(3):308. https://doi.org/10.1001/jamapediatrics.2019. 5664
- Teele DW, Klein JO, Rosner B. Epidemiology of otitis media during the first seven years of life in children in greater Boston: a prospective, cohort study. *J Infect Dis.* 1989;160(1):83-94. https://doi.org/10. 1093/infdis/160.1.83
- Shaffer AD, Ford MD, Choi SS, Jabbour N. The Impact of Timing of Tympanostomy Tube Placement on Sequelae in Children With Cleft Palate. The Cleft Palate-Craniofacial Journal. 2019;56(6):720-728. https://doi.org/10.1177/1055665618809228
- Ruohola A, Meurman O, Nikkari S, et al. Microbiology of acute otitis media in children with tympanostomy tubes: prevalences of bacteria

- and viruses. Clin Infect Dis. 2006;43(11):1417-1422. https://doi.org/10.1086/509332
- Bluestone CD, Stephenson JS, Martin LM. Ten-year review of otitis media pathogens. The Pediatric Infectious Disease Journal. 1992;11(Supplement):S7-11. https://doi.org/10.1097/00006454-199208001-00002
- Schilder AGM, Chonmaitree T, Cripps AW, et al. Otitis media. Nat Rev Dis Prim. 2016;2:1-19. https://doi.org/10.1038/nrdp.2016.63
- Ayukekbong JA, Ntemgwa M, Atabe AN. The threat of antimicrobial resistance in developing countries: causes and control strategies. Antimicrob Resist Infect Control. 2017;6(1):1-8. https://doi.org/10.1186/ s13756-017-0208-x
- Van Dyke MK, Pirçon JY, Cohen R, et al. Etiology of acute otitis media in children less than 5 years of age: a pooled analysis of 10 similarly designed observational studies. *Pediatr Infect Dis J.* 2017;36(3):274-281. https://doi.org/10.1097/INF.000000000001420
- Littorin N, Ahl J, Uddén F, Resman F, Riesbeck K. Reduction of Streptococcus pneumoniae in upper respiratory tract cultures and a decreased incidence of related acute otitis media following introduction of childhood pneumococcal conjugate vaccines in a Swedish county. BMC Infect Dis. 2016;16(1):1-8. https://doi.org/10.1186/s12879-016-1750-5
- Davies TA, Yee YC, Goldschmidt R, Bush K, Sahm DF, Evangelista A. Infrequent occurrence of single mutations in topoisomerase IV and DNA gyrase genes among US levofloxacin-susceptible clinical isolates of *Streptococcus pneumoniae* from nine institutions (1999-2003).
 J Antimicrob Chemother. 2006;57(3):437-442. https://doi.org/10. 1093/jac/dki487
- Chen DK, McGeer A, de Azavedo JC, Low DE. Decreased susceptibility of Streptococcus pneumoniae to fluoroquinolones in Canada. Canadian bacterial surveillance network. N Engl J Med. 1999;341(4):233-239. https://doi.org/10.1056/NEJM199907223410403
- Arens A. Treatment of acute otitis media in children under 2 years of age. J Emerg Med. 2011;40(6):722-723. https://doi.org/10.1016/j. iemermed.2011.04.009
- Oves M, Aslam M, Rauf MA, et al. Antimicrobial and anticancer activities of silver nanoparticles synthesized from the root hair extract of *Phoenix dactylifera*. *Mater Sci Eng C*. 2018;89(March):429-443. https://doi.org/10.1016/j.msec.2018.03.035
- Rai MK, Deshmukh SD, Ingle AP, Gade AK. Silver nanoparticles: the powerful nanoweapon against multidrug-resistant bacteria. J Appl Microbiol. 2012;112(5):841-852. https://doi.org/10.1111/j.1365-2672.2012.05253.x
- Kim JS, Kuk E, Yu KN, et al. Antimicrobial effects of silver nanoparticles. *Nanomedicine: Nanotechnology, Biology and Medicine*. 2007;3(1):95-101. https://doi.org/10.1016/j.nano.2006.12.001
- Murray RG, Steed P, Elson HE. The location of the mucopeptide in sections of the cell wall of Escherichia Coli and other gram-negative bacteria. Can J Microbiol. 1965;11:547-560. https://doi.org/10.1139/m65-072
- Qing Y, Cheng L, Li R, et al. Potential antibacterial mechanism of silver nanoparticles and the optimization of orthopedic implants by advanced modification technologies. *International Journal of Nanomedicine*. 2018; 13:3311-3327. https://doi.org/10.2147/ijn.s165125
- Ravindra S, Murali Mohan Y, Narayana Reddy N, Mohana RK. Fabrication of antibacterial cotton fibres loaded with silver nanoparticles via "Green Approach". Colloids and Surfaces A: Physicochemical and Engineering Aspects. 2010;367(1-3):31-40. https://doi.org/10.1016/j.colsurfa.2010.06.013
- Budama L, Çakır BA, Topel Ö, Hoda N. A new strategy for producing antibacterial textile surfaces using silver nanoparticles. *Chemical Engineering Journal*. 2013;228:489-495. https://doi.org/10.1016/j.cej. 2013.05.018
- Shockman GD, Barrett JF. Structure, function, and assembly of cell walls of gram-positive bacteria. Annu Rev Microbiol. 1983;37:501-527. https://doi.org/10.1146/annurev.mi.37.100183.002441

- Gupta P, Bajpai M, Bajpai SK. Textile technology: investigation of antibacterial properties of silver nanoparticle-loaded poly (acrylamide-co-itaconic acid)-grafted cotton fabric. J Cotton Sci. 2008;12(3): 280-286.
- Manke A, Wang L, Rojanasakul Y. Mechanisms of Nanoparticle-Induced Oxidative Stress and Toxicity. *BioMed Research International*. 2013;2013:1-15. https://doi.org/10.1155/2013/942916
- Roy A, Bulut O, Some S, Mandal AK, Yilmaz MD. Green synthesis of silver nanoparticles: biomolecule-nanoparticle organizations targeting antimicrobial activity. RSC Advances. 2019;9:(5)2673-2702. https://doi.org/10.1039/c8ra08982e
- Hamida RS, Ali MA, Goda DA, Khalil MI, Al-Zaban MI. Novel biogenic silver nanoparticle-induced reactive oxygen species inhibit the biofilm formation and virulence activities of methicillin-resistant *Staphylococ*cus aureus (MRSA) strain. Front Bioeng Biotechnol. 2020;8(May):1-14. https://doi.org/10.3389/fbioe.2020.00433
- Samuel MS, Jose S, Selvarajan E, Mathimani T, Pugazhendhi A. Biosynthesized silver nanoparticles using bacillus amyloliquefaciens; application for cytotoxicity effect on A549 cell line and photocatalytic degradation of p-nitrophenol. J Photochem Photobiol B Biol. 2020; 202(August 2019):111642. https://doi.org/10.1016/j.jphotobiol. 2019.111642
- Tian J, Wong KKY, Ho CM, et al. Topical delivery of silver nanoparticles promotes wound healing. *Chem Med Chem*. 2007;2(1): 129-136. https://doi.org/10.1002/cmdc.200600171
- Santoro CM, Duchsherer NL, Grainger DW. Minimal In Vitro Antimicrobial Efficacy and Ocular Cell Toxicity from Silver Nanoparticles. NanoBiotechnology. 2007;3(2):55-65. https://doi.org/10.1007/s12030-008-9007-z
- Totaro P, Rambaldini M. Efficacy of antimicrobial activity of slow release silver nanoparticles dressing in post-cardiac surgery mediastinitis. *Interact Cardiovasc Thorac Surg.* 2009;8(1):153-154. https://doi.org/10.1510/icvts.2008.188870
- Austin LA, Kang B, Yen CW, El-Sayed MA. Plasmonic Imaging of Human Oral Cancer Cell Communities during Programmed Cell Death by Nuclear-Targeting Silver Nanoparticles. *Journal of the American Chemical Society*. 2011;133(44):17594-17597. https://doi.org/10.1021/ja207807t
- He X, Peng C, Qiang S, et al. Less is more: Silver-AIE core@shell nanoparticles for multimodality cancer imaging and synergistic therapy. *Biomaterials*. 2020;238:119834. https://doi.org/10.1016/j.biomaterials.2020.119834
- He Di, Garg Shikha, Waite T. David. H2O2-Mediated Oxidation of Zero-Valent Silver and Resultant Interactions among Silver Nanoparticles, Silver Ions, and Reactive Oxygen Species. *Langmuir*. 2012;28(27):10266-10275. https://doi.org/10.1021/la300929g
- 32. Aabdallah M, Bayoumy A, Ibrahim A. Antimicrobial activity and synergistic antimicrobial potential of silver nanoparticles against microbial contaminants isolated from pharmaceutical production areas. *Res J Appl Biotechnol.* 2019;5(1):86-98. https://doi.org/10.21608/rjab.2019.76899
- Alkawareek MY, Bahlool A, Abulateefeh SR, Alkilany AM. Synergistic antibacterial activity of silver nanoparticles and hydrogen peroxide. PLoS One. 2019;14(8):1-12. https://doi.org/10.1371/journal.pone. 0220575
- Hoare TR, Kohane DS. Hydrogels in drug delivery: Progress and challenges. *Polymer*. 2008;49(8):1993-2007. https://doi.org/10.1016/j.polymer.2008.01.027
- Michida N, Hayashi M, Hori T. Comparison of event related potentials with and without hypnagogic imagery. *Psychiatry Clin Neurosci*. 1998; 52(2):145-147. https://doi.org/10.1111/j.1440-1819.1998.tb00997.x
- Moawad FA, Ali AA, Salem HF. Nanotransfersomes-loaded thermosensitive in situ gel as a rectal delivery system of tizanidine HCl: preparation, in vitro and in vivo performance. *Drug Delivery*. 2017;24(1):252-260. https://doi.org/10.1080/10717544.2016. 1245369

- Liu Y, Wang X, Liu Y, Di X. Thermosensitive In Situ Gel Based on Solid Dispersion for Rectal Delivery of Ibuprofen. AAPS PharmSciTech. 2018;19(1):338-347. https://doi.org/10.1208/s12249-017-0839-5
- Koffi AA, Agnely F, Ponchel G, Grossiord JL. Modulation of the rheological and mucoadhesive properties of thermosensitive poloxamer-based hydrogels intended for the rectal administration of quinine. Eur J Pharm Sci. 2006;27(4):328-335. https://doi.org/10.1016/j.ejps. 2005.11.001
- Sridhar V, Wairkar S, Gaud R, Bajaj A, Meshram P. Brain targeted delivery of mucoadhesive thermosensitive nasal gel of selegiline hydrochloride for treatment of Parkinson's disease. *Journal of Drug Targeting*. 2018;26(2):150-161. https://doi.org/10.1080/1061186x. 2017.1350858
- Mura P, Mennini N, Nativi C, Richichi B. In situ mucoadhesivethermosensitive liposomal gel as a novel vehicle for nasal extended delivery of opiorphin. Eur J Pharm Biopharm. 2018;122(October 2017):54-61. https://doi.org/10.1016/j.ejpb.2017.10.008
- Mirza MA, Panda AK, Asif S, et al. A vaginal drug delivery model. Drug Delivery. 2016;23(8):3123-3134. https://doi.org/10.3109/10717544. 2016.1153749
- Rençber S, Karavana SY, Şenyiğit ZA, Eraç B, Limoncu MH, Baloğlu E. Mucoadhesive in situ gel formulation for vaginal delivery of clotrimazole: formulation, preparation, and in vitro/in vivo evaluation. Pharm Dev Technol. 2017;22(4):551-561. https://doi.org/10.3109/ 10837450.2016.1163385
- Giuliano E, Paolino D, Fresta M, Cosco D. Mucosal Applications of Poloxamer 407-Based Hydrogels: An Overview. *Pharmaceutics*. 2018; 10(3):159. https://doi.org/10.3390/pharmaceutics10030159
- 44. Rana Amit Kumar, Upadhyay Deepak, Yadav Akanksha, Prasad Surendra. Correlation of Tympanic Membrane Perforation with Hearing Loss and Its Parameters in Chronic Otitis Media: An Analytical Study. Indian Journal of Otolaryngology and Head & Neck Surgery. 2020;72(2):187-193. https://doi.org/10.1007/s12070-019-01740-9
- Marchisio P, Esposito S, Baggi E, et al. Prospective evaluation of the aetiology of acute otitis media with spontaneous tympanic membrane perforation. Clin Microbiol Infect. 2017;23(7):486.e1-486.e6. https:// doi.org/10.1016/j.cmi.2017.01.010
- Mirzaei A, Janghorban K, Hashemi B, Bonyani M, Leonardi SG, Neri G. Characterization and optical studies of PVP-capped silver nanoparticles. *Journal of Nanostructure in Chemistry*. 2017;7(1):37-46. https://doi.org/10.1007/s40097-016-0212-3
- Swinehart James H.. On the Oxidation of Vanadium(II) by Oxygen and Hydrogen Peroxide. *Inorganic Chemistry*. 1965;4(7):1069-1070. https://doi.org/10.1021/ic50029a034
- Starner Timothy D., Zhang Niu, Kim GunHee, Apicella Michael A., McCray Paul B. Haemophilus influenzaeForms Biofilms on Airway Epithelia. American Journal of Respiratory and Critical Care Medicine. 2006;174(2):213-220. https://doi.org/10.1164/rccm.200509-1459oc
- Barbosa JO, Rossoni RD, Vilela SFG, et al. Streptococcus mutans can modulate biofilm formation and attenuate the virulence of Candida Albicans. PLoS One. 2016;11(3):1-16. https://doi.org/10.1371/ journal.pone.0150457
- Quintero Moreno Beatriz, Araque María, Mendoza Evelyn. Evaluation of Two Supplemented Culture Media for Long-Term, Room-Temperature Preservation ofStreptococcus pneumoniaeStrains. *BioMed Research International*. 2017;2017:1-9. https://doi.org/10.1155/ 2017/1218798
- 51. Yang Rong, Sabharwal Vishakha, Okonkwo Obiajulu S., Shlykova Nadya, Tong Rong, Lin Lily Yun, Wang Weiping, Guo Shutao, Rosowski John J., Pelton Stephen I., Kohane Daniel S.. Treatment of otitis media by transtympanic delivery of antibiotics.

- Science Translational Medicine. 2016;8(356):356ra120-356ra120. https://doi.org/10.1126/scitranslmed.aaf4363
- Giano Michael C., Ibrahim Zuhaib, Medina Scott H., Sarhane Karim A., Christensen Joani M., Yamada Yuji, Brandacher Gerald, Schneider Joel P.. Injectable bioadhesive hydrogels with innate antibacterial properties. *Nature Communications*. 2014;5:(1):https://doi.org/10.1038/ncomms5095
- Jiménez Pérez ZE, Mathiyalagan R, Markus J, et al. Ginseng-berry-mediated gold and silver nanoparticle synthesis and evaluation of their in vitro antioxidant, antimicrobial, and cytotoxicity effects on human dermal fibroblast and murine melanoma skin cell lines. Int J Nanomed. 2017;12:709-723. https://doi.org/10.2147/IJN. S118373
- Dai Tianjiao, Wang Changping, Wang Yuqing, Xu Wei, Hu Jingjing, Cheng Yiyun. A Nanocomposite Hydrogel with Potent and Broad-Spectrum Antibacterial Activity. ACS Applied Materials & Interfaces. 2018;10(17):15163-15173. https://doi.org/10.1021/acsami. 8b02527
- Dong Ruonan, Zhao Xin, Guo Baolin, Ma Peter X.. Self-Healing Conductive Injectable Hydrogels with Antibacterial Activity as Cell Delivery Carrier for Cardiac Cell Therapy. ACS Applied Materials & Interfaces. 2016;8(27):17138-17150. https://doi.org/10.1021/acsami.6b04911
- Manikam Vemal Raja, Cheong Kuan Yew, Razak Khairunisak Abdul. Chemical reduction methods for synthesizing Ag and Al nanoparticles and their respective nanoalloys. *Materials Science and Engineering: B*. 2011;176(3):187-203. https://doi.org/10.1016/j.mseb.2010.11.006
- Sun Y, Liu Y, Guizhe Z, Zhang Q. Effects of hyperbranched poly(amido-amine)s structures on synthesis of Ag particles. J Appl Polym Sci. 2008;107(1):9-13. https://doi.org/10.1002/app.26132
- Cloutier Caroline R., Alfantazi Akram, Gyenge Elod. Physicochemical Properties of Alkaline Aqueous Sodium Metaborate Solutions. *Journal* of Fuel Cell Science and Technology. 2007;4(1):88-98. https://doi.org/ 10.1115/1.2393310
- Zhang Zongtao, Zhao Bin, Hu Liming. PVP Protective Mechanism of Ultrafine Silver Powder Synthesized by Chemical Reduction Processes. Journal of Solid State Chemistry. 1996;121:(1):105-110. https://doi.org/ 10.1006/issc.1996.0015
- Chou Kan-Sen, Ren Chiang-Yuh. Synthesis of nanosized silver particles by chemical reduction method. *Materials Chemistry and Physics*. 2000;64:(3):241-246. https://doi.org/10.1016/s0254-0584(00) 00223-6
- Sadeghi B, Pourahmad A. Effects of protective agents (PVA & PVP) on the formation of silver nanoparticles. Int J Nanosci Nanotechnol. 2008;4(1):3-12.
- 62. Magdassi Shlomo, Bassa Amal, Vinetsky Yelena, Kamyshny Alexander. Silver Nanoparticles as Pigments for Water-Based Ink-Jet Inks. Chemistry of Materials. 2003;15(11):2208-2217. https://doi.org/10.1021/cm021804b
- Xu Y, Li S, Yue X, Lu W. Review of silver nanoparticles (AgNPs)cellulose antibacterial composites. *BioRes*. 2018;13(1):2150-2170.
- Pabisch S, Feichtenschlager B, Kickelbick G, Peterlik H. Effect of interparticle interactions on size determination of zirconia and silica based systems - a comparison of SAXS, DLS, BET, XRD and TEM. Chem Phys Lett. 2012;521:91-97. https://doi.org/10.1016/j.cplett. 2011.11.049
- Fissan Heinz, Ristig Simon, Kaminski Heinz, Asbach Christof, Epple Matthias. Comparison of different characterization methods for nanoparticle dispersions before and after aerosolization. *Analytical Methods*. 2014;6:(18):7324. https://doi.org/10.1039/c4ay01203h
- Beal J, Farny NG, Haddock-Angelli T, et al. Robust estimation of bacterial cell count from optical density. *Commun Biol.* 2020;3(1):512. https://doi.org/10.1038/s42003-020-01127-5

- Reimche JL, Kirse DJ, Whigham AS, Swords WE. Resistance of nontypeable Haemophilus influenzae biofilms is independent of biofilm size. Pathog Dis. 2017;75(1):1-11. https://doi.org/10.1093/femspd/ ftw112
- Pericone CD, Overweg K, Hermans PWM, Weiser JN. Inhibitory and bactericidal effects of hydrogen peroxide production by *Streptococcus* pneumoniae on other inhabitants of the upper respiratory tract. *Infect Immun.* 2000;68(7):3990-3997. https://doi.org/10.1128/IAI.68.7. 3990-3997.2000
- Carlsson J, Iwami Y, Yamada T. Hydrogen peroxide excretion by oral streptococci and effect of lactoperoxidase-thiocyanate-hydrogen peroxide. *Infect Immun.* 1983;40(1):70-80. https://doi.org/10.1128/iai. 40.1.70-80.1983
- Thomas EL, Pera KA. Oxygen metabolism of Streptococcus mutans: uptake of oxygen and release of superoxide and hydrogen peroxide. J Bacteriol. 1983;154(3):1236-1244. https://doi.org/10.1128/jb.154. 3.1236-1244.1983
- 71. Banas JA. Virulence properties of *Streptococcus mutans*. *Front Biosci*. 2004;9(June):1267-1277. https://doi.org/10.2741/1305
- Kashyap Nilotpol, Katlam Tulsi, Avinash Alok, Kumar Brij, Kulshrestha Reena, Das Pooja. Middle Ear Infection in Children and Its Association with Dental Caries. Medicine and Pharmacy Reports. 2018;https://doi.org/10.15386/cjmed-1043
- Baldeck JD, Marquis RE. Targets for hydrogen-peroxide-induced damage to suspension and biofilm cells of *Streptococcus mutans*. Can J Microbiol. 2008;54(10):868-875. https://doi.org/10.1139/ w08-078
- 74. Li Dejian, Nie Wei, Chen Liang, Miao Yingke, Zhang Xu, Chen Fancheng, Yu Bin, Ao Rongguang, Yu Baoqing, He Chuanglong. Fabrication of curcumin-loaded mesoporous silica incorporated polyvinyl pyrrolidone nanofibers for rapid hemostasis and antibacterial treatment. RSC Advances. 2017;7(13):7973-7982. https://doi.org/10.1039/c6ra27319j
- Setiyorini Y., Lou X., Pintowantoro S.. The Influence of Temperature and Drug Concentrations Prednisolone in NIPAAm Copolymer. Procedia Chemistry. 2012;4:336-342. https://doi.org/10.1016/j. proche.2012.06.047

- Vrettakos Panayotis A., Dear Steven P., Saunders James C.. Middle ear structure in the chinchilla: A quantitative study. *American Journal* of Otolaryngology. 1988;9:(2):58-67. https://doi.org/10.1016/s0196-0709(88)80009-7
- Yeo Chun Kiat, Vikhe Yogesh Shankar, Li Peng, Guo Zanru, Greenberg Peter, Duan Hongwei, Tan Nguan Soon, Chan-Park Mary B.. Hydrogel Effects Rapid Biofilm Debridement with ex situ Contact-Kill to Eliminate Multidrug Resistant Bacteria in vivo. ACS Applied Materials & Interfaces. 2018;10:(24):20356-20367. https://doi.org/ 10.1021/acsami.8b06262
- Guo Y, Wang S, Du H, Chen X, Fei H. Silver ion-histidine interplay switches peptide hydrogel from antiparallel to parallel β-assembly and enables controlled antibacterial activity. *Biomacromolecules*. 2019; 20(1):558-565. https://doi.org/10.1021/acs.biomac.8b01480
- Haidari Hanif, Kopecki Zlatko, Sutton Adam T., Garg Sanjay, Cowin Allison J., Vasilev Krasimir. pH-Responsive "Smart" Hydrogel for Controlled Delivery of Silver Nanoparticles to Infected Wounds. Antibiotics. 2021;10:(1):49. https://doi.org/10.3390/ antibiotics10010049
- Reithofer Michael R., Lakshmanan Anupama, Ping Andy T.K., Chin Jia M., Hauser Charlotte A.E.. In situ synthesis of size-controlled, stable silver nanoparticles within ultrashort peptide hydrogels and their antibacterial properties. *Biomaterials*. 2014;35:(26):7535-7542. https:// doi.org/10.1016/j.biomaterials.2014.04.102

SUPPORTING INFORMATION

Additional supporting information may be found in the online version of the article at the publisher's website.

How to cite this article: Ma X, Lang J, Chen P, Yang R. Silver nanoparticles as an effective antimicrobial against otitis media pathogens. *AIChE J*. 2021;67(12):e17468. doi: 10.1002/aic.17468